Pergamon

Journal of Structural Geology, Vol. 16, No. 4, pp. 555 to 570, 1994
Elsevier Science Ltd
Printed in Great Britain
0191-8141/94 $6.00+0.00

0191-8141(93)E0013-B

Constrictional strain in a non-coaxial shear zone: implications for fold and rock fabric development, central Mojave metamorphic core complex, California

JOHN M. FLETCHER and JOHN M. BARTLEY

Department of Geology and Geophysics, 717 William Browning Building, University of Utah, Salt Lake City, UT 84112-1183, U.S.A.

(*Received* 3 *February* 1993; *accepted in revised form* 16 *November* 1993)

Abstract—Finite strain and fold analyses of footwall mylonites in the central Mojave metamorphic core complex (CMMCC) reveal two distinct deformation paths that generated non-coaxial constrictional strain. The first path, recorded in the Waterman Hills, accomplishes constrictional strain through the formation of *L*-tectonites at the grain scale. The second path, recorded in the Mitchel Range, involves a combination of plane strain at the grain scale and *Y*-axis shortening through syn-mylonitic folding.

The ductile shear zone in the Waterman Hills is approximately 500 m thick and is developed entirely within a Miocene syn-kinematic granodiorite. Strain magnitude decreases structurally downward. The mylonites contain abundant NE-directed non-coaxial microstructures yet are *L*-tectonites. R_f/ϕ analysis of quartz-ribbon grain shapes indicate prolate strains (K=6) and bulk chemical data suggest that mylonitization was isochemical or involved volume loss. Therefore, ductile shearing in the Waterman Hills involved true constrictional strain at the grain scale.

Immediately to the southeast in the Mitchel Range, the lateral continuation of the shear zone is more than 1000 m thick and primarily involves lithologically heterogeneous pre-Tertiary basement. The mylonitic fabric comprises a well-developed foliation and NE-trending stretching lineation. R_f/ϕ strain analysis was applied to grain shapes of cataclasized and strongly altered garnet porphyroclasts in a peraluminous granite. In contrast to the Waterman Hills, finite strains in these *L*–*S*-tectonites approximate plane strain (K = 1.1). However, the mylonitic fabric is strongly folded about axes uniformly oriented subparallel to the stretching lineation. The coaxial folds range from open to isoclinal. We interpret the folds to have nucleated with axes parallel to the stretching lineation during mylonitization and to have accomplished *Y*-axis shortening in the shear zone. Macroscopic folds of the brittle detachment spatially correspond to open folds in the ductile shear zone, suggesting that *Y*-axis shortening continued after the fault zone had reached the brittle regime.

Corrugations and folds oriented subparallel to the transport direction are characteristic features of fault zones in Cordilleran metamorphic core complexes. Therefore, constrictional strain may be common in core complexes. Strain compatibility with upper plate rocks in core complexes may be maintained by *Y*-axis shortening along conjugate strike slip faults. A nearly uniaxial stress field ($\sigma_3 < \sigma_2 \approx \sigma_1$) is consistent with most of the structures formed in Basin and Range extension and could generate the observed constrictional strain.

INTRODUCTION

DEFORMATION paths in shear zones are commonly interpreted in terms of the ideal shear zone model (Ramsay & Graham 1970, Ramsay 1980). In the model, ductile shear zones are the kinematic equivalent of brittle fault zones: the shear zone is bounded by rigid blocks that are displaced relative to each other. As a result, deformation is dominated by simple shear. This geometry requires plane strain, i.e. no true strain along the intermediate principal strain axis (*Y*-axis) of the shear zone. Apparent departures from plane strain are accomplished through dilatation of the shear zone perpendicular to its walls (Ramsay & Wood 1973). Apparent flattening strains are produced by volume loss and apparent constriction by volume gain.

We report field and laboratory studies of mylonites in the extensional shear zone of the central Mojave metamorphic core complex (CMMCC). The results indicate true *Y*-axis shortening that cannot be interpreted in terms of the ideal shear zone model. We argue that, besides accomplishing relative displacement of the bounding blocks, crustal-scale ductile shear zones may record a more complete deformational expression of the large-scale tectonic regime. In other words, we suggest that a single ductile shear zone may accomplish strains that could only be produced by a network of brittle faults with some combination of dip-slip and strike-slip displacements.

The basin-and-dome geometry of the brittle–ductile faults in Cordilleran metamorphic core complexes is the result of the superposition of two upright fold sets (Spencer 1982, Yin 1991, Yin & Dunn 1992). One set comprises long-wavelength folds with axes that trend perpendicular to the movement direction. Most workers agree that this folding of the fault zone occurs in response to tectonic denudation and isostatic rebound of the footwall (Spencer 1984, Buck 1988, Hamilton 1988, Wernicke & Axen 1988, Bartley *et al.* 1990, Reynolds & Lister 1990). These structures clearly overprint mylonitization and active displacement across the fault zone and are not considered further in this paper. The second set consists of shorter-wavelength folds oriented parallel to the movement direction. The genesis of these folds is controversial. Some workers interpret the folds to form as primary corrugations in the fault zone (John 1987,

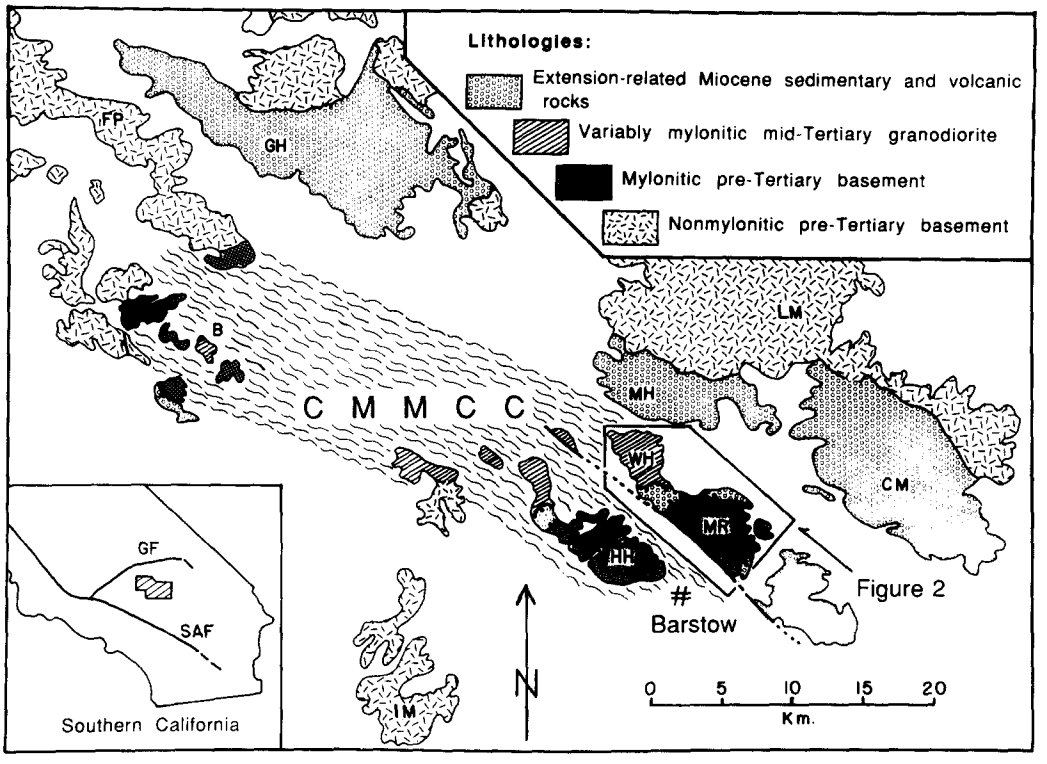

Fig. 1. Schematic geologic map of the central Mojave metamorphic core complex (CMMCC). Area ornamented with wavy lines is alluvium-covered but inferred to be underlain by Miocene mylonite. B—Buttes, CM—Calico Mountains, FP—Fremont Peak, GH—Gravel Hills, HH—Hinkley Hills, IM—Iron Mountain, LM—Lane Mountain, MH—Mud Hills, MR—Mitchel Range, WH—Waterman Hills, SAF—San Andreas Fault, GF—Garlock Fault.

Spencer & Reynolds 1991). Others argue that the movement-parallel folds formed by secondary folding of an originally sub-planar fault zone (Spencer 1982, Yin 1991, Yin & Dunn 1992). Our data support the latter theory and indicate that folding occurred during active displacement across the brittle–ductile fault zone in the CMMCC. We interpret this folding and extensional faulting to reflect a large-scale constrictional strain regime in which horizontal extension occurred along the azimuth of fault slip and shortening occurred along vertical and horizontal axes perpendicular to the azimuth of fault slip.

This study presents finite strain and fabric analyses from two along-strike segments of the ductile shear zone in the CMMCC that record two different constrictional strain paths. We reevaluate existing models for syn-mylonitic folding and outline deformational processes that occur in a shear zone undergoing constrictional strain. Finally, we suggest that constrictional strain may be a common product of extensional tectonism.

CENTRAL MOJAVE METAMORPHIC CORE COMPLEX

The CMMCC is characterized by a NE-directed detachment fault system that can be traced 40 km along strike (Fig. 1). Normal-sense displacement across the fault zone separated regional pre-Tertiary lithologic markers in the hanging wall and footwall by approximately 40–60 km (Glazer *et al.* 1989, Martin & Walker 1991). This extension occurred between 23 and 18 Ma: mylonitization involved 23 ± 0.9 Ma dacite dikes (Walker *et al.* 1990) and the 18–30 Ma Barstow Formation (Burke *et al.* 1982, MacFadden *et al.* 1990) was deposited post-kinematically in the rift basin (Glazner *et al.* 1989). This study focuses on exposures of the ductile shear zone at the southeastern end of the core complex in the Waterman Hills and Mitchel Range (Fig. 2).

The detachment fault system is laterally continuous in this area and composed of four main structural components. Brittle faults, including the detachment and upper-plate faults, form the structurally highest elements. The detachment juxtaposes mid-Tertiary volcanic and sedimentary rocks in the hangingwall with mylonitized crystalline basement in the footwall. A zone of penetrative cataclasis extends 50–100 m below the detachment-fault surface. Ultramylonites that record extreme grain-size reduction and significant chemical alteration (Glazner & Bartley 1991) occur in a 5–10 m thick zone immediately below the detachment fault. Finally, greenschist-facies mylonites occur in the ductile shear zone that reaches a thickness in excess of 1000 m. As observed in all Cordilleran metamorphic core complexes, brittle deformational fabrics overprint ductile fabrics.

The brittle–ductile fault system does not change from the Waterman Hills to the Mitchel Range except for the character of mylonitization in the ductile shear zone. In the Mitchel Range mylonitization primarily affected heterogeneous pre-Tertiary basement that consists of interleaved meta-sedimentary and meta-igneous rocks. Meta-sedimentary units include quartzite, pelite and marble which are tentatively correlated with late

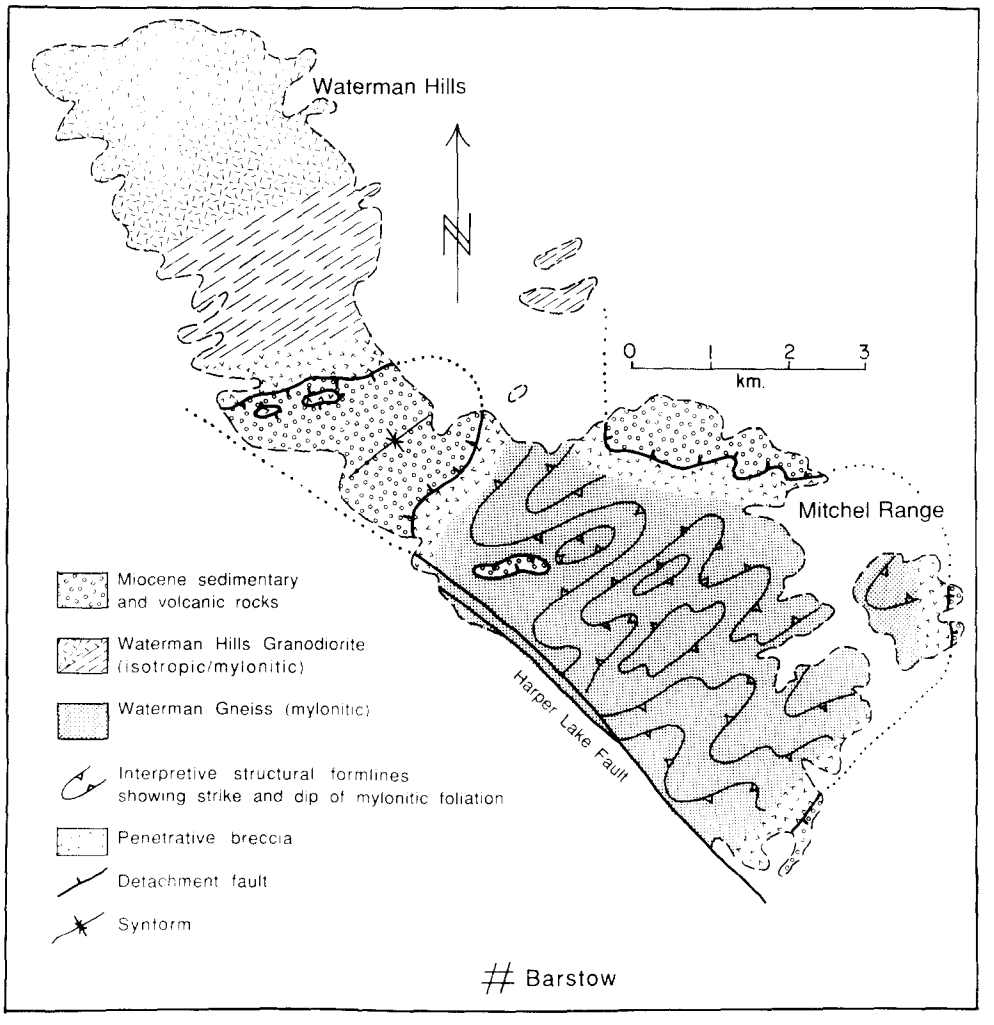

Fig. 2. Schematic geologic map of the Waterman Hills and Mitchel Range. Miocene granodiorite in the Waterman Hills contains an *L*-tectonite fabric. Pre-Tertiary rocks in the Mitchel Range are *L*–*S*-tectonites folded about axes subparallel to the stretching lineation.

Proterozoic–Paleozoic Cordilleran miogeoclinal strata (Stewart & Poole 1975, Kiser 1981). Meta-igneous rocks range in composition from gabbro to leucogranite with hornblende metagabbro forming the dominant lithology in the range. Although these rocks are almost completely overprinted by Tertiary greenschist-facies mylonitization, porphyroclasts in pelitic rocks preserve a relict upper amphibolite-facies assemblage of garnet + biotite + muscovite + quartz ± kyanite ± sillimanite ± staurolite from an earlier, probably Mesozoic, thermotectonic event. The issue of distinguishing strains associated with Mesozoic deformation from mid-Tertiary mylonitization is discussed later.

In contrast to the lithologically heterogeneous mylonites in the Mitchel Range, the ductile shear zone in the Waterman Hills only affects a medium- to coarse-grained granodiorite pluton, dated by the U/Pb zircon method at about 22–23 Ma (Glazner *et al.* 1992). Primary minerals in the granodiorite include euhedral cyclically-zoned plagioclase, quartz, biotite and minor hornblende with poikilitic orthoclase overgrowing all other phases. Late myrmekite partially replaces orthoclase. Most of the important differences in character between the two shear zone segments are consistent with the interpretation that the granodiorite was emplaced during mylonitization. The remainder of this paper outlines and compares the structural evolution of these two shear zone segments.

SYN-MYLONITIC DEFORMATIONAL FABRICS

The monolithologic ductile shear zone in the Waterman Hills is approximately 500 m thick and displays a strong strain gradient with structural level. The granodiorite is essentially isotropic and undeformed in the structurally lowest exposures and develops a progressively more intense mylonitic fabric upward toward the brittle detachment (Bartley *et al.* 1990, Glazner & Bartley 1991). Lithologic markers such as aplite dikes contain the mylonitic fabric but are not rotated into parallelism with it.

The ductile shear zone in the Mitchel Range is much thicker: its lower boundary is not exposed in about 1000 m of structural relief. However, the shear zone contains macroscopic blocks of relatively unmylonitized rock, indicating that strain is heterogeneous within the zone. Most of the shear zone is characterized by mylonitic

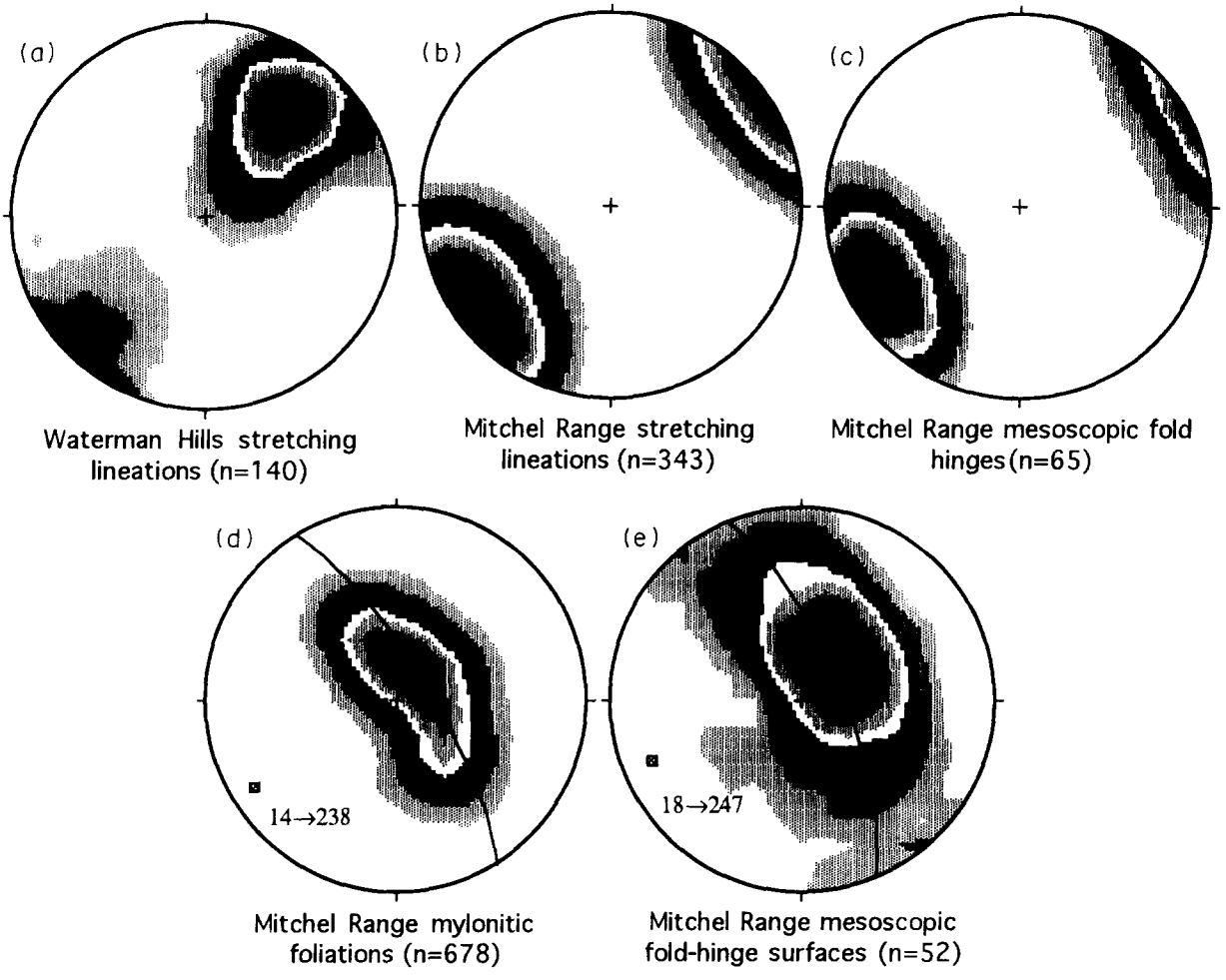

Fig. 3. Mylonitic fabrics from the Waterman Hills and Mitchel Range. Data contoured by Kamb method on equal-area stereonets. (a) Contour interval = 2.0 sigma, (b) contour interval = 5.0 sigma, (c) contour interval = 2.2 sigma, (d) pole to great-circle girdle is 14–238. Contour interval = 3.5 sigma, (e) pole to great-circle girdle is 18–247. Contour interval = 1.2 sigma.

gneissic banding. Lithologic markers, which include early Miocene dacite dikes, are generally completely rotated into parallelism with the mylonitic fabric. Only sparse, as-yet undated felsite dikes are cross-cut by the fabric but not fully transposed. Rotation and transposition of compositional layering occurred largely through synmylonitic folding which is discussed in a later section.

The mesoscopic character of the mylonitic fabric differs in the two shear zone segments. The mylonites in the Waterman Hills segment are nearly pure *L*-tectonites that contain no measurable foliation (Bartley *et al.* 1990, Glazner & Bartley 1991). The stretching lineation plunges northeast and southwest (Fig. 3a). The Mitchel Range segment is predominantly composed of *L*–*S*-tectonites that are defined by a prominent stretching lineation and an equally well developed foliation (Dokka 1989). However, strongly rodded *L*-tectonites are exposed locally. The stretching lineation in the Mitchel Range is subparallel to that in the Waterman Hills (Fig. 3b).

Despite the significant differences in the character of the mylonitic fabric, both shear zone segments record a significant component of NE-directed non-coaxial strain. Rotational kinematic indicators are abundant and include *S*–*C* fabrics, *C′* shear bands, sigma- and delta-type augen, mica fish arrays and domino-block rotations in fractured hornblende, feldspar and garnet porphyroclasts (Bartley *et al.* 1990, Dokka 1989). Mylonitization in both segments involved transitional brittle–plastic deformation mechanisms (Bartley *et al.* 1990): quartz is dynamically recrystallized and shows evidence for both dislocation creep and dislocation glide; feldspars are cataclastically deformed and syn-kinematically replaced by cryptocrystalline aggregates of quartz, white mica, and plagioclase; and micas are kinked and sheared into arrays of fish with separations larger than the dimensions of the standard thin section. $^{40}Ar/^{39}Ar$ release spectra constrain peak temperatures of mylonitization to 300–400°C; phengitic white mica yields a disturbed spectrum of about 52 Ma while biotite is totally reset to 20–22 Ma (J. M. Bartley & W. J. Taylor unpublished data).

In summary, similarities in the stretching lineation orientation, NE-directed shear-sense and deformation mechanisms of mylonitization suggest that the laterally contiguous shear zone segments in the Waterman Hills and Mitchel Range developed coevally in the same deformational regime. The ductile shear zone in the Waterman Hills displays a continuous upward increase

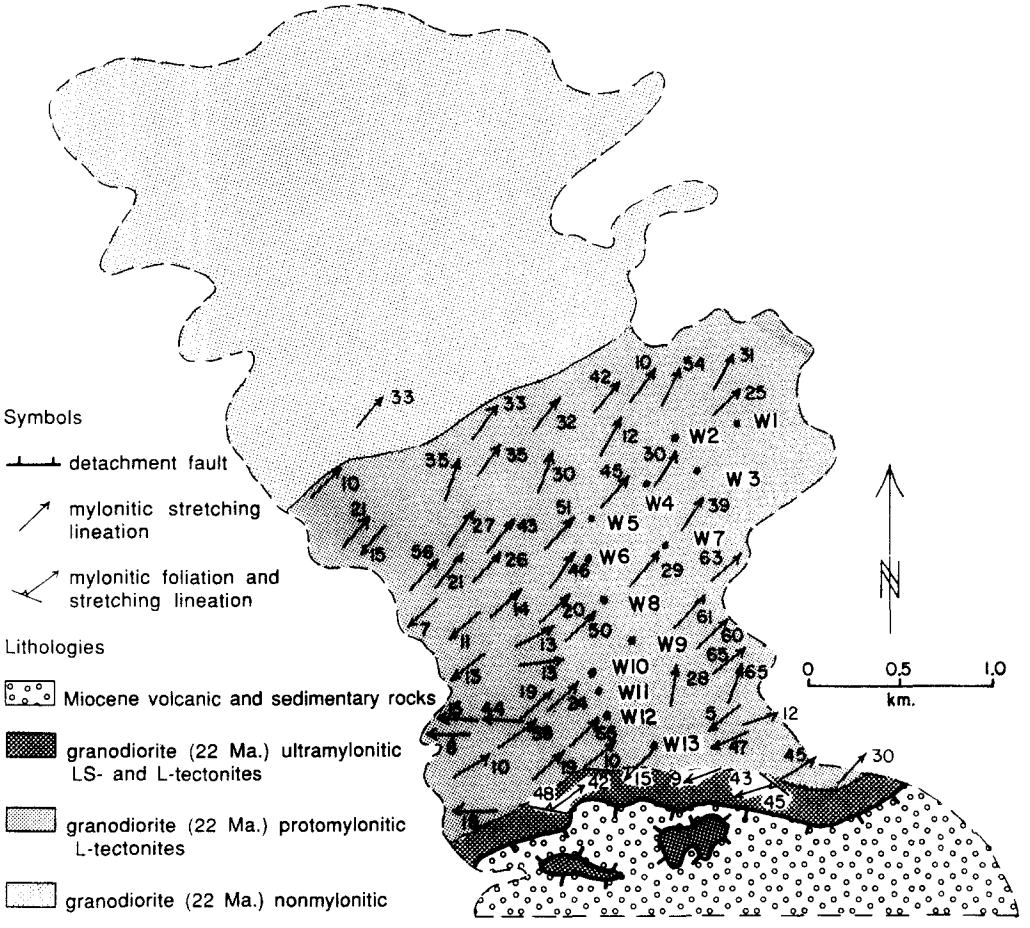

Fig. 4. Geologic map of the Waterman Hills showing locations of samples collected for the R_f/ϕ strain analysis (W1–W13). Samples collected near the detachment yield the highest strain magnitudes.

in fabric intensity but, aside from a thin zone of ultramylonite beneath the detachment fault, strain magnitudes were not high enough to transpose mesoscopic compositional markers. In the Mitchel Range segment, variations in fabric intensity occur without any simple relationship to structural position, and compositional markers are typically transposed into parallelism with the mylonitic fabric. Qualitatively, the *L–S*-tectonites in the Mitchel Range appear to record higher strain magnitudes and a larger flattening component than *L*-tectonites in the Waterman Hills.

FINITE STRAIN ANALYSIS

Methodology

Several techniques were considered for measuring finite strain in the metaigneous mylonites, including magnetic susceptibility anisotropy (AMS), porphyroclast reconstruction, R_f/ϕ analysis of distorted primary-grain shapes and normalized-Fry analysis of primary-grain distributions. We concluded that R_f/ϕ analysis of grain shapes yielded the most reliable results. Strain determinations using AMS were problematic. Mean susceptibilities in the granodiorite were too low (of the order of 10^{-8} cgs units) for precise AMS measurements with the available instrument. Mylonitic gabbro in the Mitchel Range segment yielded mean susceptibilities between 10^{-3}–10^{-5} cgs units and both prolate and oblate anisotropy ellipsoids. In general, increases in mean susceptibility are positively correlated with increases in the degree of anisotropy, suggesting that both the shape and magnitude of the susceptibility anisotropy reflect variations in magnetic mineralogy and not variations in finite strain (Borradaile 1987, Borradaile & Sarvas 1990).

Strain determinations using porphyroclast reconstruction might have been attempted on the Mitchel Range mylonites which contain abundant microcracked and boudinaged feldspar porphyroclasts with quartz fibers defining separations. However, the technique was not pursued because of observed microstructures that could cause erroneous strain estimates. Quartz fibers between widely separated fragments were commonly completely attenuated and thus made a large fraction of the total extensional strain difficult to recognize. Strong deflections of the external foliation around porphyroclasts suggest that they resisted shortening strains. Finally, strain accommodated in the cryptocrystalline alteration products of feldspar could not be measured in such reconstructions.

In the Waterman Hills segment, the study was restricted to the early Miocene granodiorite. Samples were obtained at different structural levels to document the vertical strain gradient (Fig. 4). In order to compare

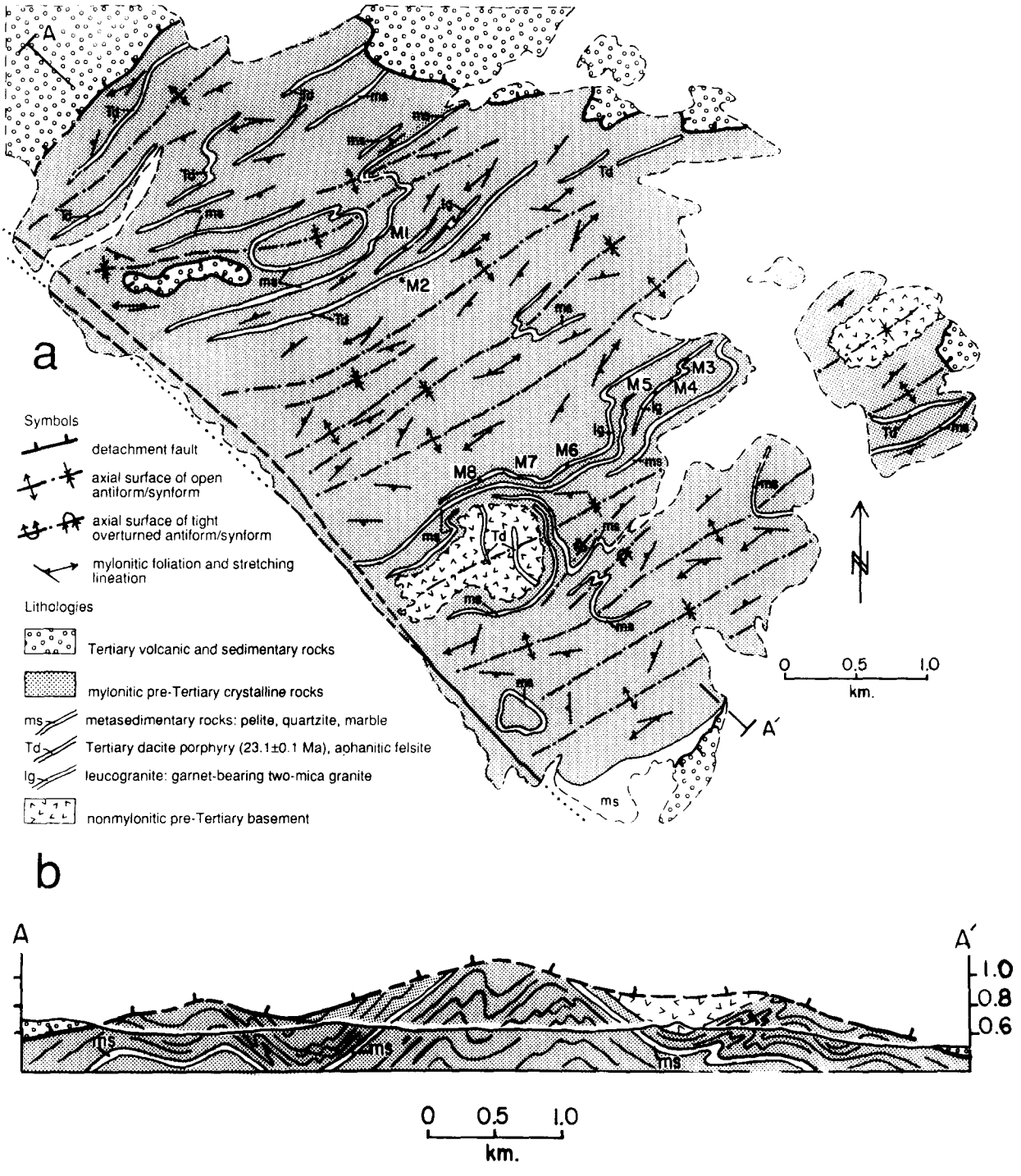

Fig. 5. (a) Geologic map of the Mitchel Range showing locations of leucogranite samples collected from the R_f/ϕ strain analysis. Cross-section A–A′ drawn perpendicular to movement. Antiformal and synformal undulations in the brittle detachment surface correspond to type 1 folds in the ductile shear zone.

finite strains between the two areas, a two-mica garnet-bearing granite with a similar quartz:feldspar ratio to the granodiorite was examined in the lithologically heterogeneous Mitchel Range. The pre-Tertiary granite occurs as a one meter thick unit that can be traced for several kilometers along strike. Therefore, samples from the Mitchel Range were collected from essentially one structural level in the same zone (Fig. 5).

Deformed primary quartz grains were the most distinctive markers in the granodiorite from the Waterman Hills (Figs. 6a & c). However, quartz markers in the peraluminous granite from the Mitchel Range could not be used because higher strain magnitudes made it difficult to distinguish pressure shadows from primary quartz ribbons. Well-developed quartz pressure shadows suggest that silica was either added to the bulk rock or transferred out of primary quartz grain domains. Thus, quartz grains in the granite were affected by volumetric strains that would be difficult to assess. Instead, garnet porphyroclasts that were penetratively cataclasized and

strongly altered to fine-grained aggregates of chlorite, biotite and opaques were abundant and made excellent markers (Figs. 6b & d). We infer that these fine-grained micaceous aggregates deformed primarily as passive markers because the external foliation in the matrix is only weakly deflected around them. However, it is likely that alteration and cataclasis occurred at some point during deformation and that the garnet porphyroclasts may not record strain from the earliest stages of deformation. This inaccuracy should only affect the absolute magnitude of the strain determinations if the axial ratios of the three-dimensional strain ellipsoid remained constant during progressive deformation. A possible factor that could affect the character of the measured finite strain is boudinage of the markers due to stretching parallel to the X axis. This would cause the maximum elongation to be underestimated and shift the measured finite strain ratios toward the flattening field.

Sample preparation for R_f/ϕ and normalized-Fry analyses involved cutting large (20–30 cm) hand samples along three mutually perpendicular faces subparallel to the XY, YZ and XZ principal planes and tracing the strain markers on transparent overlays on the wetted slab surfaces. The tracings were then digitized. A least-squares best-fit ellipse was calculated for each marker outline as well as its relative position and orientation. Approximately 50–120 grains were measured on each principal plane. From these data scatter plots for the normalized Fry (Ersley 1988) and R_f/ϕ (Dunnet 1969) methods were generated.

Tectonic strains were determined from the chi-squared minima of the R_f/ϕ analyses (Peach & Lisle 1979). The chi-squared tests typically yielded initial-ellipticity estimates of 1.72. Symmetrical R_f/ϕ plots indicate no recognizable pre-existing preferred orientation of strain markers in either the Miocene granodiorite or the pre-Tertiary granite. Finite strains determined from the normalized Fry technique were primarily used to check the R_f/ϕ estimates. The precision of these results was poor but they crudely agree with the R_f/ϕ determinations. This agreement suggests that the finite strains recorded by the markers used in the R_f/ϕ grain-shape analysis are roughly equal to those of the matrix and that the strain markers deformed passively. Lastly, the R_f/ϕ strain estimates from three subperpendicular planes were used to calculate a finite-strain ellipsoid according to the modified least-squares technique of Owens (1984). These results are summarized in Table 1.

Results

The L-tectonites in the Waterman Hills yield strongly prolate finite strain ellipsoids that plot well within the field of apparent constriction (Fig. 7). The data define a radial trend with a K value of about 6. Finite-strain magnitude is systematically related to structural level in the shear zone: larger strain magnitudes are recorded at progressively higher levels. Glazner & Bartley (1991) interpret the volumetric strain in these mylonites to be negligible because they found no significant differences in the whole-rock geochemistry of mylonitized and unmylonitized granodiorite; only the ultramylonites adjacent to the brittle detachment underwent large volume changes. Additionally, quartz-filled tensile cracks are rare suggesting that closed-system pressure solution was not an important deformation mechanism and that volume was also conserved in grain domains. Therefore, the L-tectonites record true constrictional strain which requires shortening along both the Y and the Z principal strain axes.

Although the mylonitized granite in the Mitchel Range crops out only at one structural level in the shear zone, measured strain in the L–S-tectonites varies sufficiently to define a radial trend on a Flinn diagram near plane strain (Fig. 7). Strain magnitudes in the Mitchel Range segment are high and marker ellipticities in the XZ principal plane are commonly greater than 50:1. Bulk-rock volumetric strains in the mylonitized peraluminous granite are difficult to assess because its undeformed protolith has not been identified. However, whole-rock geochemistry of mylonitized and unmylonitized gabbro in the Michel Range indicates either isochemical behavior or volume loss, similar to the Waterman Hills granodiorite (A. F. Glazner unpublished data). Volumetric strain also could have occurred in garnet grain domains as a result of the breakdown of garnet to chlorite and biotite. We are currently in the process of quantifying this component of strain through characterization of phase chemistry and metamorphic reactions but presently it remains undetermined. Although volumetric strains are not well constrained in the Mitchel Range mylonites, it is unlikely that they are sufficient to cause the difference in strain paths between the Waterman Hills and Mitchel Range. In other words, an anisotropic Z axis volume loss of nearly 85% is required to produce an apparent plane-strain path from a true constrictional-strain path with a K value of 6. We present microstructural evidence below which suggests that the Mitchel Range mylonites record no Y axis strain and that the R_f/ϕ strain estimates accurately reflect the true tectonic strains.

Microstructural indicators of finite strain

Microstructures in thin sections cut subparallel to the principal planes of finite strain were compared to the strain paths predicted from R_f/ϕ determinations. Specifically, we identified how extension and contraction were accomplished at the grain scale along the X and Z axes, respectively, and searched for comparable microstructures along the Y axis. The sign of elongation along the Y axis qualitatively indicates whether the true finite strain is constrictional, flattening or plane strain. Microstructures that indicate contraction include concentration of mica and deflection of external foliation around competent porphyroclasts, preferred orientations of mica and elongate quartz subgrains in the mylonitic matrix, and domino-style shear displacements

across microcracks. Dilation across microcracks, microboudinage, pressure shadows and secondary quartz fibers indicate directions of extension. Qualitative differences in strain magnitude are defined by the relative degree of grain-size reduction, deformation-enhanced chemical alteration and microstructural development.

The sheared granodiorite in the Waterman Hills segment has a protomylonitic fabric that lacks penetrative grain-size reduction. The *L*-tectonite fabric is defined largely by grain elongations accomplished by the intracrystalline deformation mechanisms described above. However, the bulk rock aggregate also is cut by discrete zones of high shear strain that we call microshear surfaces. These zones are defined by finely recrystallized grains of quartz and mica, and commonly link biotite fish into arrays. The microshear zones are as thin as 10–30 microns but generally become thicker and more abundant as the intensity of the deformational fabric increases.

Microstructural evidence for prolate strain is most readily observed in the *YZ* plane, on which elongate quartz subgrains commonly are oriented parallel to the margins of the nearest feldspar porphyroclast and biotite grains show no preferred orientation. Microshear surfaces in the *YZ* plane are short, discontinuous and form an anastomosing network with only a weak preferred orientation parallel to the *Y* axis. On the *XY* plane, high-strain zones are more continuous and oriented at the small angle to the *X* axis. Evidence for *Y* axis shortening in the *XY* plane includes: concentrations of mica on the margins of feldspar porphyroclasts, and domino-style shear displacements across microcracks (Fig. 6e). The longest shear surface traces occur on the *XZ* principal plane where they form evenly spaced sets parallel to the *X* axis.

Chemical alteration and mylonitization are more penetrative in the granitic *L–S*-tectonites from the Mitchel Range. Cryptocrystalline replacement products after feldspar occupy up to 60% of the rock volume and commonly form long tails in the pressure shadows of porphyroclasts. Microcracks in feldspar porphyroclasts record wide separations and are filled with fibrous secondary quartz.

Microstructures in the Mitchel Range tectonites suggest that no finite elongation occurred along the *Y* axis. On the *XY* plane, microcracks in feldspar occur either perpendicular to the *X* axis or as conjugate sets at a high angle to the *X* axis. However, regardless of the crack orientation, quartz fibers defining the displacement vector always are parallel to the *X* axis (Fig. 6f). In contrast, flattening of porphyroclasts by shear displacements across microcracks and narrowing of fiber bundles away from widely separated porphyroclasts commonly were observed on the *XZ* plane. Lastly, although the *YZ* plane displays a well defined foliation, no pressure shadows were observed around the porphyroclast margins. Therefore, microstructures that demonstrate shortening along the *Z* axis and extension along the *X* axis are absent along the *Y* axis, corroborating the R_f/ϕ estimates of plane strain in the Mitchel Range mylonites.

MESOSCOPIC AND MACROSCOPIC COMPONENTS OF FINITE STRAIN: SYN-MYLONITIC FOLDS

R_f/ϕ and microstructural estimates of finite strain indicate that the *L–S*-tectonites in the Mitchel Range record a substantially larger flattening component and higher strain magnitudes than the *L*-tectonites in the Waterman Hills. However, grain-scale finite strain is only part of the total macroscopic strain that a shear zone records. The main differences between the two shear zone segments can be explained by considering the tectonic history and larger-scale deformation of the mylonitic fabric in the shear zone.

The difference in strain magnitude may reflect syn-kinematic emplacement of the granodiorite in the Waterman Hills. The granodiorite cuts transposed compositional layering in mylonitic pre-Tertiary rocks but is itself mylonitized. Further, the timing of rift-basin evolution overlaps with the age of the granodiorite. Current age constraints indicate that the extensional basins in this area were initiated by 24 Ma (W. J. Taylor *et al.* unpublished $^{40}AR/^{39}Ar$ data) and extension continued until 18.5 Ma (Dokka 1989, Glazner *et al.* 1989). This indicates that the granodiorite was emplaced during extension and may have only recorded some of the strain that transposed compositional layering in its wall rocks.

The contrast between constrictional vs plane strain may reflect differences in scale-dependent strain partitioning. The only mesoscopic and macroscopic structural feature in Waterman Hills tectonites is the increase in strain magnitude toward the detachment which does not affect the constrictional character of the finite strain. Therefore, the total macroscopic finite strain in this shear zone segment was accomplished at the grain scale. In contrast, the *L–S*-tectonites in the Mitchel Range are strongly affected by mesoscopic and macroscopic syn-mylonitic folding. These folds include a broad spectrum of geometries but all have hinges oriented subparallel to the SW-plunging mylonitic stretching lineation (Figs. 3b & c). Poles to both mylonitic layering and axial surfaces of mesoscopic folds define great-circle girdles with best-fit fold axes that also plunge to the southwest (Figs. 3d & e).

The coaxial syn-mylonitic folds are classified according to their style and relationship to the mylonitic fabric. Type 1 folds are upright open folds of the mylonitic layering (Fig. 8a). These folds typically are symmetric, have interlimb angles greater than 90° and lack an associated upright axial-planar cleavage. Type 2 folds are strongly asymmetric, have interlimb angles less than 90° and contain an inclined axial-planar mylonitic foliation that cuts through the short limb of the fold pair (Fig. 8b). Type 3 folds include recumbent isoclinal folds to which the mylonitic foliation is axial planar (Fig. 8c), and sheath folds which are much less common (Fig. 8d).

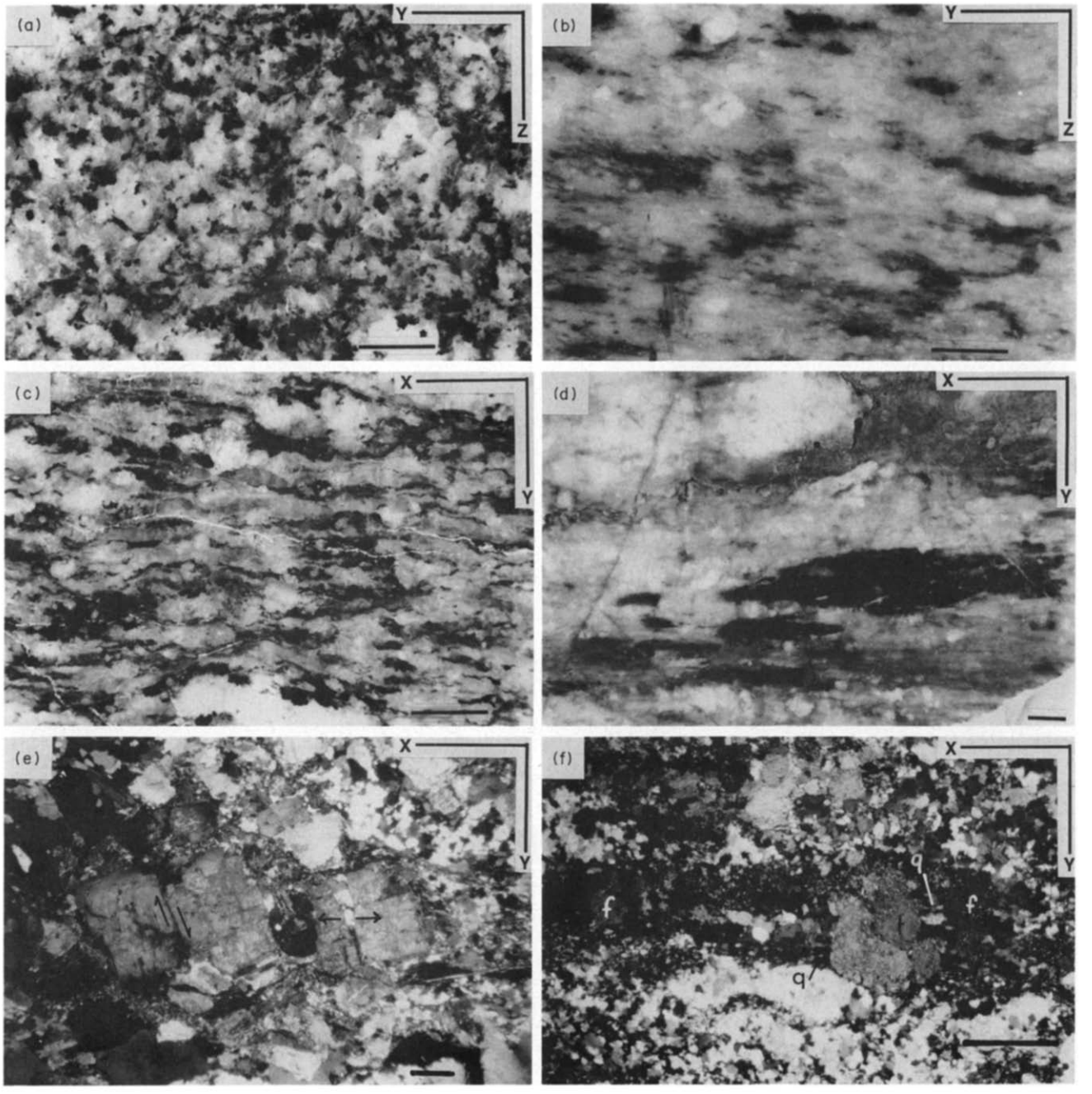

Fig. 6. Rock slabs and photomicrographs cut subparallel to the principal planes of finite strain. (a) & (b) Granodiorite from the Waterman Hills, sample W-11. Quartz is gray, biotite is black and feldspar is white. Note isotropic character of mylonitic fabric in *YZ* plane (a) (scale bar = 5 mm). (c) & (d) Peraluminous granite from the Mitchel Range, sample M-7. Strain markers are altered garnet porphyroclasts (black), feldspar is white and quartz if light gray. Note well-developed planar foliation in *YZ* plane (c) (scale bar—5 mm). (e) *XY* plane of Waterman Hills *L*-tectonite, sample W-11. *X* axis extension is defined by quartz-filled tensile cracks. *Y* axis contraction is defined by shear displacement across microcracks, and by concentrations of recrystallized biotite on margins of feldspar porphyroclasts that lie perpendicular to the *Z* axis (scale bar—1.0 mm). (f) *XY* plane of Mitchel Range *L*–*S*-tectonite, sample M-5. Fibrous quartz (**q**) defines tensile separation of feldspar porphyroclasts (**f**). No evidence for *Y* axis strain (scale bar = 1.0 mm).

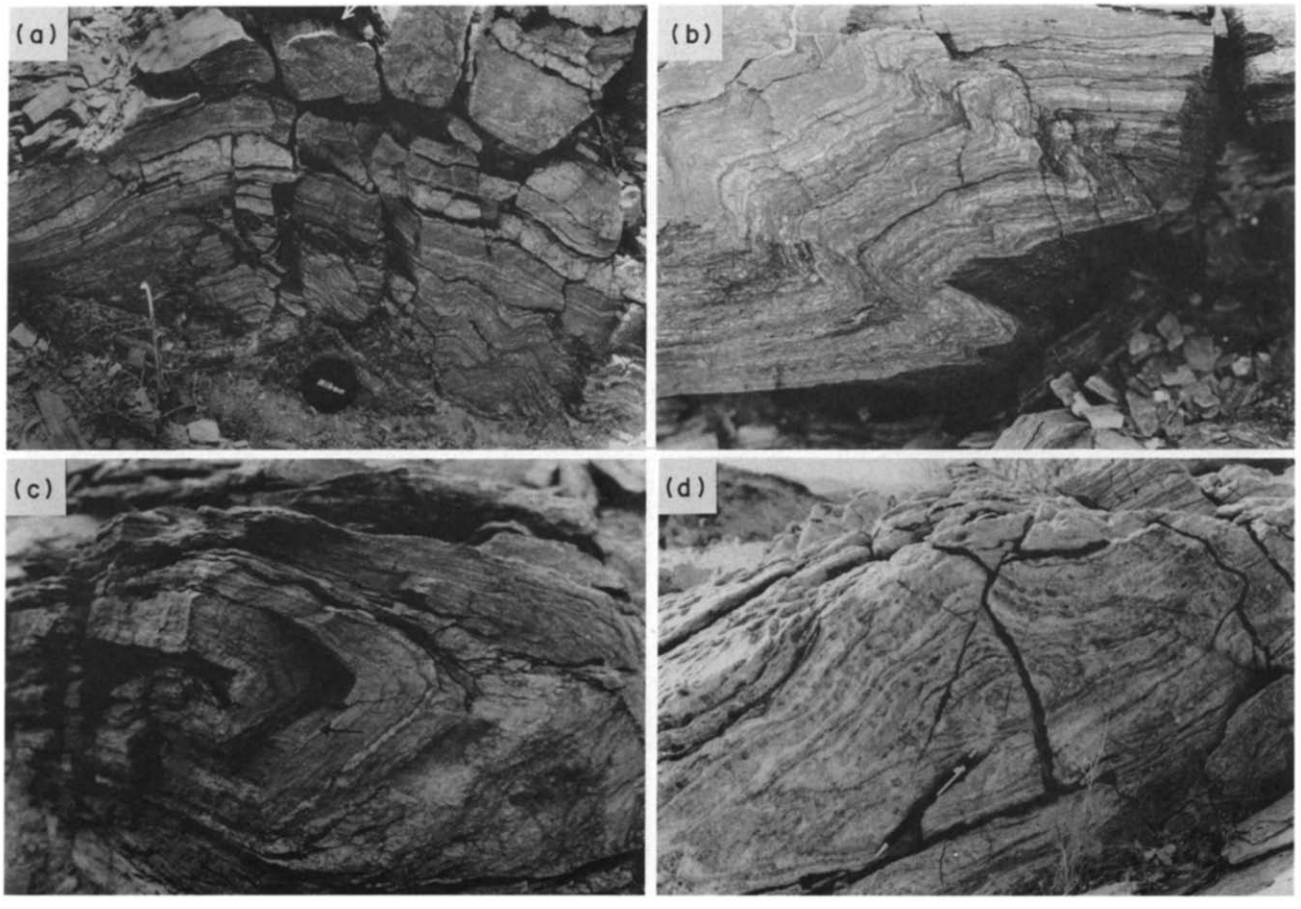

Fig. 8. Syn-mylonitic fold geometries in the Mitchel Range. (a) Type 1 upright gentle fold of mylonitic layering. (b) Type 2 recumbent asymmetric fold with axial planar cleavage cutting short limb of the fold pair. (c) Type 3 recumbent tight fold. Mylonitic foliation is the axial planar cleavage. (d) Type 3 sheath fold. Aspect ratio of fold closure is 2–4. Arrows point to surfaces containing the stretching lineation.

Table 1. Strain data from the Waterman Hills and Mitchel Range. Principal stretches were calculated assuming constant volume strain. Data averages are arithmetic means except for K values. Average K values were calculated by fitting a straight line through the origin (1,1) and minimizing deviations in R_{xy}. Sample locations are shown in Figs. 4 and 5

Sample	R_{xy}	R_{yz}	R_{xz}	K	S_x	S_y	S_z
Waterman Hills							
W1	2.64	1.09	2.88	18.22	1.97	0.74	0.68
W2	3.42	1.01	3.45	242.00	2.28	0.67	0.66
W3	2.26	1.78	4.02	1.62	2.09	0.92	0.52
W4	2.86	1.28	3.66	6.64	2.19	0.76	0.60
W5	2.94	1.26	3.70	7.46	2.22	0.75	0.60
W6	2.45	1.74	4.26	1.96	2.19	0.89	0.51
W7	3.58	1.20	4.30	12.90	2.49	0.69	0.58
W8	2.84	1.76	5.00	2.42	2.42	0.85	0.48
W9	3.44	1.80	6.19	3.05	2.77	0.81	0.45
W10	4.16	1.24	5.16	13.17	2.78	0.67	0.54
W11	5.22	1.10	5.74	42.40	3.11	0.60	0.54
W12	4.59	1.96	9.00	3.74	3.46	0.75	0.38
W13	4.19	1.83	7.67	3.84	3.18	0.76	0.41
Average	3.43	1.47	5.00	6.01	2.55	0.76	0.54
Mitchel Range							
M1	7.45	5.17	38.52	1.55	6.60	0.89	0.17
M2	3.53	4.27	15.07	0.77	3.76	1.07	0.25
M3	7.68	6.26	48.08	1.27	7.17	0.93	0.15
M4	5.77	4.45	25.68	1.38	5.29	0.92	0.21
M5	4.28	5.38	23.03	0.75	4.62	1.08	0.20
M6	5.45	5.55	30.25	0.98	5.48	1.01	0.18
M7	5.45	4.30	23.44	1.35	5.04	0.92	0.21
M8	5.26	4.29	22.57	1.29	4.91	0.93	0.22
Average	5.61	4.96	28.33	1.11	5.36	0.97	0.20

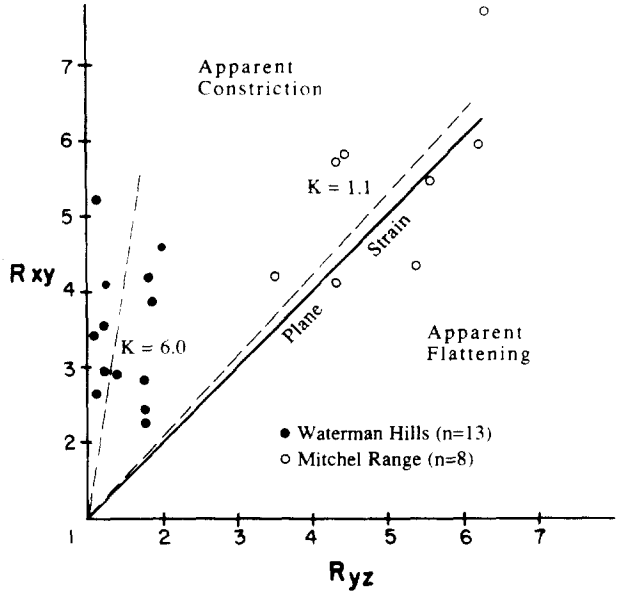

Fig. 7. Flinn diagram of R_f/ϕ strain data.

Sheath folds typically have hinge angles less than 10° and eye-shaped closures with aspect ratios of 2–4 in down-plunge sections.

The dominant macroscopic structure of the shear zone in the Mitchel Range is a range-scale type 1 antiform that contains smaller wavelength (approximately 2 km) type 1 folds (Fig. 5). The brittle detachment cuts folded mylonitic layering but it is also broadly warped into a similar range-scale antiform (Fig. 5b). In the northwest part of the Mitchel Range, klippe occur near the axial trace of a shorter wavelength type 1 synform which suggests that the brittle detachment contains antiformal and synformal undulations that are also broadly congruent with the shorter wavelength type 1 folds in the shear zone (Fig. 5b). These cross-cutting relationships indicate that much of the type 1 folding occurred in the ductile regime but we speculate that the undulations of the detachment reflect the continued growth of type 1 folds in the brittle regime.

Mechanisms by which folds develop with axes parallel to the stretching lineation in shear zones can be divided into two main categories. The first involves progressive rotation of fold axes that nucleate at high angles to the stretching lineation. Alternatively, folds may form with axes that initially lie subparallel to the stretching lineation. Cobbold & Quinquis (1980) provided theoretical and experimental models for fold nucleation and hinge-line rotation during progressive simple shear. Their model 1 has become a widely accepted explanation of the formation of sheath folds and distribution of fold hinges in shear zones. However, several observations limit the application of this model to the Mitchel Range shear zone. (1) Open type 1 folds which are abundant and appear to record the initial stages of fold formation could not have undergone significant hinge-line rotation. (2) Fold hinges plot a cluster and do not form the predicted great-circle distribution. (3) Skjernaa (1989) demonstrated that sheath folds with hinge angles less than 20° should have aspect ratios of 35:1 if formed by this mechanism. Clearly, this prediction does not fit the observed sheath fold geometries in the Mitchel Range.

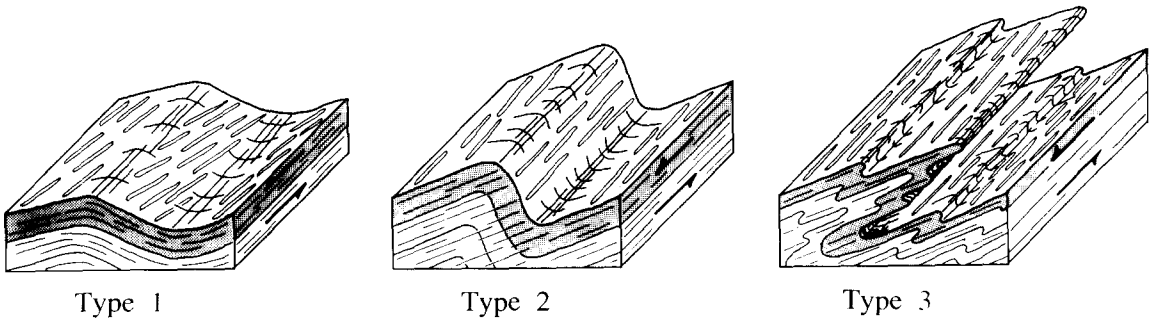

Fig. 9. Interpreted sequential development of folds as defined by the three styles of folds observed in the Mitchel Range. Type 1 folds nucleated with axes subparallel to the stretching direction in response to Y axis shortening. With continued shearing, type 1 folds developed into type 2 and 3 folds as outlined by Skjernaa (1989).

Skjernaa (1989) modeled the consequences of overprinting horizontal simple shear on upright open folds with axes subparallel to the slip vector. The predicted fold geometries and hinge distributions match well the observed structures in the Mitchel Range shear zone. According to her model, if the upright progenitor fold axis is parallel to the slip vector, the top portion of the fold will be displaced relative to the bottom but no change in fold geometry will occur (Skjernaa 1989, fig. 5b). However, if the progenitor fold axis lies in the slip plane but oblique to the slip direction, subsequent shearing produces recumbent asymmetric folds similar to type 2 and 3 folds (Skjernaa 1989, fig. 5c). For a given shear strain, the resultant fold geometry becomes tighter as the initial angle between fold axis and slip direction increases. Initial angles less than 15° are required to create type 2 folds when a shear strain of 10 is applied (Skjernaa 1989). Finally, sheath folds with geometries similar to those seen in the Mitchel Range are formed when the progenitor fold axis is oblique to the slip plane and rotates into the shortening field with subsequent shearing (Skjernaa 1989, figs. 5e & f).

In the Mitchel Range type 1 folds have the same geometry as progenitor folds of Skjernaa's (1989) model and field relationships indicate that they formed during progressive shearing. Two possible mechanisms that could create such folds include lateral displacement gradients (Coward & Potts 1983, Ridley 1986, Holdsworth 1990) or shortening along the Y axis of the shear zone in a constrictional strain regime. Lateral displacement gradients can be factorized into simple shear on two orthogonal planes with a common slip vector which Ridley (1986) terms 'thrust- and wrench-shear' components. The resultant strain is simple shear on an inclined plane that contains the common slip vector (Flinn 1979). Ridley (1986) demonstrates that folds will form with axes nearly parallel to the stretching lineation if the pre-existing layering lies parallel to the 'thrust-shear' plane. The fold axes and stretching lineation initiate at 45° to the slip vector and progressively rotate into parallelism with it. The axial surfaces of these folds are parallel to the XY plane of the resultant simple shear (Ridley 1986).

Several factors render this mechanism of fold formation in the Mitchel Range unlikely. (1) The development of upright folds requires 'wrench' shear to dominate 'thrust' shear which is highly implausible given the lack of independent evidence for wrench shear. (2) Although strain is heterogeneous in the Mitchel Range, no consistent lateral strain gradient was observed. The abrupt decrease in strain magnitude between the Mitchel Range and Waterman Hills is only an apparent gradient due to synkinematic emplacement of the granodiorite. (3) A lateral displacement gradient can not produce true constrictional strain as observed in the Waterman Hills because the resultant simple shear is, by definition, plane strain.

Syn-mylonitic folds and fabrics in the Mitchel Range are likely to have formed in response to the partitioning of constrictional strain into plane strain at the grain scale and Y axis shortening through larger-scale folding. The range of coaxial fold geometries is considered to represent a sequence in a continuous deformational process (Fig. 9). This process begins at the grain scale where deformation is dominated by simple shear. As the mylonitic fabric develops it is folded into type 1 folds. The folds become asymmetric and tighter with subsequent shearing as outlined by Skjernaa (1989). Field relationships indicate that a new axial-planar mylonitic fabric develops as the short limb of an asymmetric fold is rotated away from the XY plane of the shear zone. These type 2 folds become progressively tighter until they are completely transposed. True Y axis shortening only occurs in the earlier stages of fold formation because final fold amplification takes place by movement on the axial planar mylonitic fabric that records plane strain.

This deformational process will produce the observed fold geometries and hinge distributions in the Mitchel Range. The continuous nature of the process is reflected in the great-circle girdle distribution of poles to both the mylonitic foliation and the axial planes of the mesoscopic folds (Figs. 3d & e). Finally, lateral shortening in response to constrictional strain is consistent with the formation of L-tectonites in the Waterman Hills.

DISCUSSION

We interpret the mylonites in the Mitchel Range and Waterman Hills to record two distinct constrictional strain paths. The L-tectonites in the Waterman Hills

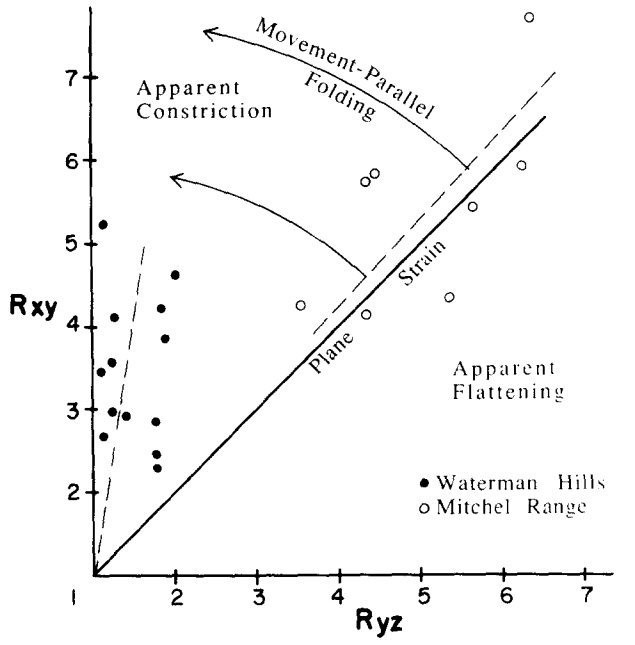

Fig. 10. Effects of macroscopic strain and tectonic history on grain-scale paths. Constrictional strain in the Waterman Hills is accomplished at the grain scale by the formation of *L*-tectonites. Constrictional strain in the Mitchel Range is accomplished by mesoscopic and macroscopic folding of *L–S*-tectonites about axes oriented subparallel to the stretching direction. Waterman Hills tectonites record lower strain magnitudes because the syn-kinematic granodiorite only recorded the later fraction of the total strain history.

accomplish non-coaxial constriction at the grain scale, whereas constrictional strain in the Mitchel Range was accomplished by movement-parallel folding of *L–S*-tectonites that record plane strain at the grain scale (Fig. 10). This interpretation raises several important questions. Why do the shear zone segments accomplish constrictional strain by two completely different deformation paths? How is *Y* axis strain compatibility maintained between the rocks in the shear zone and rocks outside the shear zone? Is bulk constrictional strain plausible in an extensional tectonic setting?

Strain paths and deformational processes

We consider three hypotheses to explain the development of two distinct strain paths in the adjacent shear zone segments. The pre-Tertiary rocks in the Mitchel Range record a Mesozoic thermotectonic event and may have contained a pre-existing deformation fabric. The Mesozoic tectonic layering may have controlled the grain-scale fabric of the superposed mylonitization. Depending on the initial orientation of the layering, it could have acted as slip surfaces for simple shear or inhibited *Y* axis contraction. The Mesozoic fabric in this region typically involves a strong subvertical gneissic layering, but on the grain scale it is statically recrystallized and equigranular (Fletcher *et al.* 1991). Thus, although the early fabric may have controlled the character of mid-Tertiary mylonitic strain at the grain scale, it should not have affected the actual R_f/ϕ and microstructural estimates of finite strain.

Alternatively, because the *L*-tectonites record lower strain magnitudes than the *L–S*-tectonites, the deformation path at the grain scale may have evolved from constrictional to plane strain. Simple shear, requiring only one slip surface and one slip direction, may be favored over other more complex strain paths at the grain scale. However, in the incipient stages of deformation, the grain-scale deformational fabric probably will reflect the bulk strain regime because inherent weaknesses in the rock are randomly oriented. For example, microshear surfaces which define the *L*-tectonite fabric in the Waterman Hills appear to have nucleated on biotite grains and the altered portions of feldspar porphyroclasts. In the initial stages of non-coaxial constriction, these inherent weaknesses can be exploited in a manner that reflects the macroscopic strain regime. However, at greenschist-facies conditions the rock contains large concentrations of minerals with a single active slip system, e.g. quartz and phyllosilicates. We hypothesize that as microlithons decrease in size and minerals develop a preferred orientation, simple shear on a single slip surface may become the dominant mode of deformation at the grain scale.

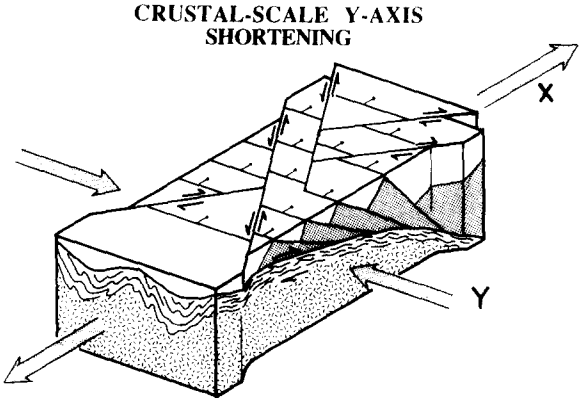

Fig. 11. Strain compatibility is maintained by *Y* axis shortening in the shear-zone bounding blocks. Possible structures include conjugate strike-slip faults and folds with axes parallel to the movement direction.

Finally, because the syntectonic granodiorite only records the later stages of mylonitization, it is possible that the strain field changed from non-coaxial plane strain before granodiorite emplacement to non-coaxial constriction after. Each of these three scenarios is consistent with our data.

Strain compatibility

The ductile shear zone in the CMMCC records true constrictional strain and therefore cannot be bounded by rigid blocks, Instead, *Y* axis shortening must occur throughout the crust in order to maintain strain compatibility with the shear zone (Ramsay and Wood 1973, Ramsay 1980). However, *Y* axis shortening in the hanging wall block need not occur immediately above the ductile shear zone but could affect rocks laterally offset from constriction in the shear zone.

Y axis shortening in the fault-zone bounding blocks is likely to occur by formation of either: (1) folds with axes parallel to the extension direction; or (2) networks of conjugate strike slip faults (Fig. 11). In the Colorado

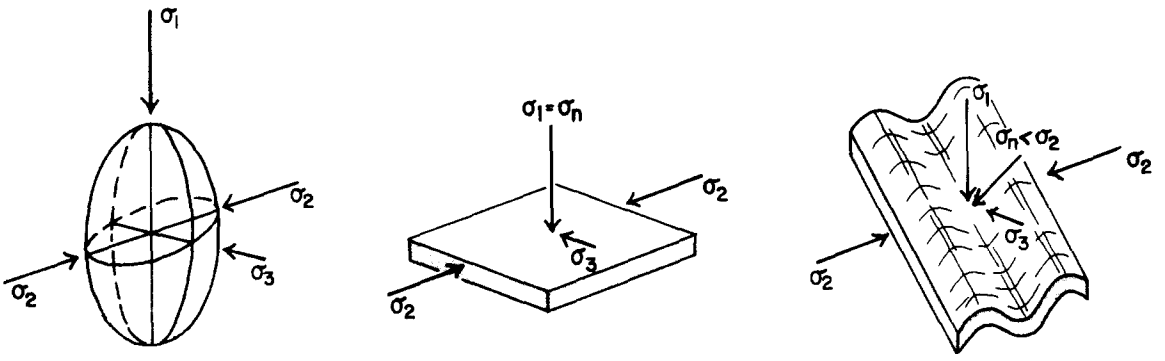

Fig. 12. Formation of folds with axes parallel to the extension direction in an Andersonian stress regime. Normal stress on a horizontal layer is equal to σ_1 and buckling in response to σ_2 is impossible. Normal stress on an inclined layer is less than σ_1 and buckling in response to σ_2 may be possible.

River Trough extensional belt, Yin (1991) documents folds with axes parallel to the movement direction in sills and mylonites in the footwall as well as in sedimentary rocks in the hanging wall. Detachment faulting in the southern Basin and Range is commonly coupled with conjugate strike-slip faults which together produce large-scale constrictional strain (Wright 1976, Wernicke *et al.* 1982, 1988, Anderson & Barnhard 1984, Glazner & Bartley 1984). Therefore, we suggest that crustal-scale shear zones such as that in the CMMCC may not be bounded by rigid blocks and consequently the finite strain need not behave according to the ideal shear zone model.

Dynamic feasibility of generating constrictional strain and folding instability

A nearly uniaxial stress field with ($\sigma_3 < \sigma_2 \approx \sigma_1$) is the simplest stress configuration that can produce constrictional strain. Theoretical considerations suggest that such a stress field is reasonable in an extensional tectonic setting. In the absence of imposed tectonic stresses, McGarr (1988) proposed that a hydrostatic state of stress ($\sigma_1 = \sigma_2 = \sigma_3$ = lithostatic load) is the most stable configuration in the crust. According to the Anderson fault theory, crustal extension occurs when compressive stresses are sufficiently reduced in one horizontal direction along the σ_3 axis. Near the surface of the Earth, σ_1 will be vertical and equal to the lithostatic load. However, the magnitude of σ_2, which is horizontal and perpendicular to the extension direction, should also remain approximately equal to the lithostatic load. Nearly uniaxial stresses are also commonly inferred from inversions of fault-slip and earthquake focal mechanism data in many extensional terranes throughout the Basin and Range (Zoback 1989).

Therefore, the principal stress axes crudely coincide with the principal strain axes on the scale of the entire extensional orogen. The crust is simultaneously extended along the subhorizontal σ_3 axis and shortened along the subvertical σ_1 axis by displacement on the detachment fault system. Additionally, the crust is shortened along the subhorizontal σ_2 axis by the formation of *L*-tectonites, movement-parallel folds and conjugate strike-slip faults.

However, on the scale of individual fault zones and tectonic blocks, the principal stress axes cannot coincide with the principal strain axes and still generate the observed structures. When modeling the formation of folds in the Colorado River detachment system, Yin (1991) demonstrated that it is possible to create buckle folds with axes parallel to the extension direction in a subhorizontal elastic sheet with nearly uniaxial tectonic stresses. Buckling instability for folds that form in response to σ_2 compression will never develop because the normal stress across the elastic sheet is σ_1 (Yin 1991). In fact, this relationship holds for other rheologies as well. Smith (1977) showed that for Newtonian and non-Newtonian media, end loads must be greater than normal stresses to generate folding instability with reasonable growth rates.

In the extensional tectonic regime, such a stress configuration can occur if the fault zone is inclined to the principal stress axes, i.e. the resolved normal stress across the zone will be less than σ_1 and σ_2 (Fig. 12). Therefore, folding instability for folds with axes parallel to the extension direction may be possible in the fault zone, as well as in any inclined layering in the extending terrane. Additionally, the fault zone must be inclined to the principal stresses to generate shear stress that drives displacement. Even when the formation of movement-parallel folds is mechanically impossible, *Y* axis shortening by conjugate strike-slip faulting could occur in the uniaxial stress field because ($\sigma_2 - \sigma_3$), the stress difference that drives strike-slip faulting, is identical to ($\sigma_1 - \sigma_3$), the stress difference that drives normal faulting.

CONCLUSIONS

(1) Non-coaxial constriction in the CMMCC was accomplished by two different deformation paths. The first path accomplished constrictional strain at the grain scale through the formation of *L*-tectonites. The second

path involved a combination of plane strain at the grain scale and Y axis shortening through syn-mylonitic folding.

(2) Syn-mylonitic folding in a shear zone that accommodates constrictional strain is characterized by the nucleation and amplification of folds with axes parallel to the stretching lineation. Folds nucleate as upright open folds and continued shearing produces recumbent tight and isoclinal folds as well as sheath folds.

(3) Corrugations in the brittle detachment of the CMMCC record Y axis shortening in the brittle regime and do not appear to be primary undulations in the fault surface.

(4) Y axis shortening outside the fault zone may be accomplished by structures such as conjugate sets of strike slip faults and folds with axes parallel to the extension direction.

(5) A nearly uniaxial stress field ($\sigma_3 < \sigma_2 \approx \sigma_1$) could generate constrictional strain and most of the structures associated with large-magnitude extension in the Basin and Range. Based on independent theoretical considerations, we suggest that uniaxial stresses may arise in extensional tectonic settings.

Acknowledgements—This project was funded by NSF grants EAR8816944 and EAR8916838. Fortran programs written by Adolph Yonkee were used throughout the quantitative strain analysis. Stereoplots were generated with Richard Allmendinger's program Stereonet 4.5a. We wish to thank Ron Bruhn for the use of his lab and expertise. Allen Glazner provided unpublished geochemical data, Mark Martin and Doug Walker provided unpublished U/Pb data, and John Bendixen, Rob Fillmore, Anke Friedrich and Andy Manning assisted in various aspects of field and laboratory work. We are grateful to Mark Brandon, Bradley Hacker and Jon Spencer for thorough reviews and comments that improved the paper.

REFERENCES

Anderson, R. E. & Barnhard, T. P. 1984. Extensional and compressional paleostresses and their relationship to paleoseismicity and seismicity, Central Sevier Valley, Utah. *U.S. geol. Surv. Open-file Rep.* **84-763**, 515–544.

Bartley, J. M., Fletcher, J. M. & Glazner, A. F. 1990. Tertiary extension and contraction of lower plate rocks in the Central Mojave Metamorphic Core Complex, southern California. *Tectonics* **9**, 521–534.

Borradaile, G. 1987. Anisotropy of magnetic susceptibility: rock composition versus strain. *Tectonophysics* **138**, 327–329.

Borradaile, G. & Sarvas, P. 1990. Magnetic susceptibility fabrics in slates: structural, mineralogical and lithological influences. *Tectonophysics* **172**, 215–222.

Buck, R. 1988. Flexural rotation of normal faults. *Tectonics* **7**, 959–973.

Burke, D. B., Hillhouse, J. W., McKee, E. H. Miller, S. T. & Morton, J. L. 1982. Cenozoic rocks in the Barstow Basin area of southern California–stratigraphic relations, radiometric ages, and paleomagnetism. *Bull. U.S. geol. Surv.* **1529-E**, 1–16.

Cobbold, P. R., & Quinquis, H. 1980. Development of sheath folds in shear regimes. *J. Struct. Geol.* **2**, 119–126.

Coward, M. P. & Potts, G. J. 1983. Complex strain patterns developed at the frontal and lateral tips to shear zones and thrust zones. *J. Struct. Geol.* **5**, 383–399.

Dokka, R. K. 1989. The Mojave Extensional Belt of southern California. *Tectonics* **8**, 363–390.

Dunnet, D. 1969. A technique of finite strain analysis using deformed elliptical particles. *Tectonophysics* **2**, 117–136.

Erslev, E. 1988. Normalized center-to-center strain analysis of packed aggregates. *J. Struct. Geol.* **10**, 201–209.

Fletcher, J. M., Martin, M. & Bendixen, J. 1991. Mid-Tertiary mylonitization and deep-seated Mesozoic contraction in the Buttes (abs.). *Cordilleran Section, Geol. Soc. Am. Abs. w. Prog.* **23**, A25.

Flinn, D. 1979. The deformation matrix and the deformation ellipsoid. *J. Struct. Geol.* **1**, 299–308.

Glazner, A. F. & Bartley, J. M. 1984. Timing and tectonic setting of Tertiary low-angle normal faulting and associated magmatism in the southwestern United States. *Tectonics* **3**, 385–396.

Glazner, A. F., & Bartley, J. M. 1991. Volume loss, fluid flow and state of strain in extensional mylonites from the central Mojave Desert, California. *J. Struct. Geol.* **13**, 587–594.

Glazner, A. F., Fletcher, J. M., Martin, M. W., Walker, J. D. & Bartley, J. M. 1992. Widespread Miocene plutonism and ductile deformation (abstract). *Eos* **73**, 548.

Glazner, A. F., Bartley, J. M. & Walker, J. D. 1989. Magnitude and significance of Miocene crustal extension in the central Mojave Desert, California. *Geology* **17**, 50–53.

Hamilton, W. 1988. Detachment faulting in the Death Valley region, California and Nevada. *Bull. U.S. geol. Surv.* **1790**, 51–85.

Holdsworth, R. E. 1990. Progressive deformation structures associated with ductile thrusts in the Moine Nappe, Sutherland, N. Scotland. *J. Struct. Geol.* **12**, 443–452.

John, B. E. 1987. Geometry and evolution of a mid-crustal extensional fault system: Chemihuevi Mountains, southeastern California. In: *Continental Extensional Tectonics* (edited by Coward, M. P., Dewey, J. F. & Hancock, P. L.). *Spec. Publs geol. Soc. Lond.* **28**, 313–335.

Kiser, N. L. 1981. Stratigraphy structure and metamorphism in the Hinkley Hills, Barstow, California. Unpublished M.S. thesis, Stanford University.

McFadden, B. J., Swisher, C. C., Updyke, N. D. & Wood 1990. Paleomagnetism, geochronology, and possible tectonic rotation of the middle Miocene Barstow Formation, Mojave Desert, Southern California. *Bull. geol. Soc. Am.* **102**, 478–493.

Martin, M. W. & Walker, J. D. 1991. Upper Precambrian–Paleozoic paleogeographic reconstruction of the Mojave Desert, California. In: *Paleozoic Paleogeography of the Western United States—II* (edited by Cooper, J. D. & Stevens, C. H.). *Pacific Section, Soc. econ. Paleont. Miner.* **67**, 167–192.

McGarr, A. 1988. On the state of lithospheric stress in the absence of applied tectonic forces. *J. geophys. Res.* **93**, 13 609–13 617.

Owens, W. H. 1984. The calculation of a best fit ellipsoid from elliptical sections on arbitrarily oriented planes. *J. Struct. Geol.* **6**, 571–578.

Peach, C. J. & Lisle, R. J. 1979. A Fortran IV program for the analysis of tectonic strain using deformed elliptical markers. *Comput. & Geosci.* **5**, 325–334.

Ramsay, J. G. 1980. Shear zone geometry: a review. *J. Struct. Geol.* **2**, 83–99.

Ramsay, J. G. & Graham, R. H. 1970. Strain variation in shear belts. *Can. J. Earth Sci.* **7**, 786–813.

Ramsay, J. G. & Wood, D. S. 1973. The geometric effects of volume change during deformation processes. *Tectonophysics* **16**, 263–277.

Reynolds, S. J. & Lister, G. S. 1990. Folding of mylonitic zones in Cordilleran metamorphic core complexes: evidence from near the mylonitic front. *Geology* **18**, 216–219.

Ridley, J. 1986. Parallel stretching lineations and fold axes oblique to shear displacement direction—a model and observations. *J. Struct. Geol.* **8**, 647–653.

Skjernaa, L. 1989. Tubular folds and sheath folds: definitions and conceptual models for their development, with examples from the Grapesvare area, northern Sweden. *J. Struct. Geol.* **11**, 689–703.

Smith, R. B. 1977. Formation of folds, boudinage, and mullions in non-Newtonian materials. *Bull. geol. Soc. Am.* **88**, 312–320.

Spencer, J. E. 1982. Origin of folds of Tertiary low-angle fault surfaces, southeastern California and western Arizona. In: *Mesozoic–Cenozoic Tectonic Evolution of the Colorado River Region, California, Arizona, and Nevada* (edited by Frost, E. G. & Martin, D. L.). Cordilleran Publishers, San Diego, California, 123–134.

Spencer, J. E. 1984. Role of denudation in warping and uplift of low-angle normal faults. *Geology* **12**, 95–98.

Spencer, J. E. & Reynolds, S. J. 1991. Tectonics of mid-Tertiary extension along a transect through west-central Arizona. *Tectonics* **10**, 1204–1221.

Steward, J. H. & Poole, F. G. 1975. Extension of the Cordilleran miogeosynclinal belt to the San Andreas Fault, southern California. *Bull. geol. Soc. Am.* **86**, 205–212.

Walker, J. D., Bartley, J. M. & Glazner, A. F. 1990. Large-magnitude Miocene extension in the central Mojave Desert: implications for

Paleozoic to Tertiary Paleogeography and tectonics. *J. geophys. Res.* **95**, 557–569.
Wernicke, B. & Axen, G. J. 1988. On the role of isostacy in the evolution of normal fault systems. *Geology* **16**, 848–851.
Wernicke, B., Axen, G. J. & Snow, J. K. 1988. Basin and Range extensional tectonics at the latitude of Las Vegas, Nevada. *Bull. geol. Soc. Am.* **100**, 1738–1757.
Wernicke, B., Spencer, J. E., Burchfiel, B. C. & Guth, P. L. 1982. Magnitude of crustal extension in the southern Great Basin. *Geology* **10**, 499–502.
Wright, L. 1976. Late Cenozoic fault patterns and stress fields in the Great Basin and westward displacement of the Sierra Nevada block. *Geology* **4**, 489–494.
Yin, A. 1991. Mechanisms for the formation of domal and basinal detachment faults: a three-dimensional analysis. *J. geophys. Res.* **96**, 14 577–14 594.
Yin, A. & Dunn, A. F. 1992. Structural and stratigraphic development of the Whipple–Chemehuevi detachment fault system, southeastern California: implications for the geometrical evolution of domal and basinal low-angle normal faults. *Bull. geol. Soc. Am.* **104**, 659–674.
Zoback, M. L. 1989. State of stress and mofern deformation of the northern Basin and Range province. *J. geophys. Res.* **94**, 7105–7128.